STEM CELL REPORTS
Article
ISSCR
OPEN ACCESS

Microbiota from young mice restore the function of aged ISCs

Kodandaramireddy Nalapareddy,[1,*] David B. Haslam,[2] Ann-Kathrin Kissmann,[3] Theresa Alenghat,[4] Selina Stahl,[5] Frank Rosenau,[3] Yi Zheng,[1,6] and Hartmut Geiger[4,6,7,*]
[1]Division of Experimental Hematology and Cancer Biology, Cincinnati Children's Hospital Medical Center and University of Cincinnati, Cincinnati, OH 45229, USA
[2]Director, Microbial Genomics and Metagenomics Laboratory, Cincinnati Children's Hospital Medical Center and University of Cincinnati, Cincinnati, OH 45229, USA
[3]Institute of Pharmaceutical Biotechnology, Ulm University, Albert-Einstein-Allee 11, 89081 Ulm, Germany
[4]Division of Immunobiology and Center for Inflammation and Tolerance, Cincinnati Children's Hospital Medical Center and Department of Pediatrics, University of Cincinnati College of Medicine, Cincinnati, OH, USA
[5]Institute of Molecular Medicine, Ulm University, Ulm, Germany
[6]These authors contributed equally
[7]Lead contact
*Correspondence: kodandaramireddyn@gmail.com (K.N.), hartmut.geiger@uni-ulm.de (H.G.)
https://doi.org/10.1016/j.stemcr.2025.102788

SUMMARY

Homeostasis in the intestinal epithelium depends on intestinal stem cells (ISCs). A reduction in the function of ISCs, caused by a decline of canonical Wnt signaling in ISCs, contributes to a reduced regenerative potential of the aged intestine. The composition of the intestinal microbiota changes upon aging. We report here that aging-associated changes in the composition of the microbiota result in reduced canonical Wnt signaling through *Ascl2* in ISCs, which causes a decline in the regenerative potential of aged ISCs *in vivo*. We demonstrate, using microbiota transfer experiments, that interestingly, elevated levels of *Akkermansia muciniphila* in the intestine cause a reduction of *Ascl2*-mediated canonical Wnt signaling in ISCs and thus reduced regeneration of the aged epithelium. The composition of the intestinal microbiota thus plays a critical role in regulating the function of ISCs. Our data imply potential therapeutic approaches via modulation of the composition of microbiota for aging-associated changes in the function of ISCs.

INTRODUCTION

The intestinal epithelium depends on intestinal stem cells (ISCs) for maintaining homeostasis (Barker et al., 2007; Nalapareddy et al., 2022). The intestinal epithelium shows a reduced rate of turnover with age, which is at least in part due to a decline in ISC function (Nalapareddy et al., 2017; Pentinmikko et al., 2019). ISCs reside at the bottom of the cup-shaped invagination called *crypt*, flanked by differentiated Paneth cells that serve as a niche for ISCs. ISCs divide every 24 h and give rise to progenitors called transient amplifying (TA) cells. TA cells differentiate into villus comprising enterocytes, goblet cells, enteroendocrine cells, and the recently identified tuft cells. Except for Paneth cells that travel down to the crypt bottom, all other differentiated cells travel up into the villus. A cell from the crypt base takes approximately 4–5 days to reach the tip of the villus to shed into the intestinal lumen (Barker et al., 2007).

Aged ISCs show a reduced ability to self-renew and differentiate compared to young ISCs. This overall decline in regenerative capacity of ISCs results in slower recovery from damage and, therefore, renders the intestine more vulnerable to injury (Nalapareddy et al., 2017, 2022). The reduced function of aged ISCs is, in part, due to a decline in canonical Wnt signaling within ISCs, driven by lower levels of canonical Wnts in aged ISCs themselves and as well as in aged crypts (Nalapareddy et al., 2017, 2022). In addition, changes in NOTCH and mTOR (mechanisitc Target of Ripamyin) signaling have been linked to aging of ISCs (He et al., 2020; Nalapareddy et al., 2017). It was further shown that NOTUM, a Wnt deacetylase secreted from Paneth cells, also contributes to aging of ISCs. NOTUM modifies Wnts in the stem cell niche, and by this means, modulates canonical Wnt signaling in ISCs (Pentinmikko et al., 2019). Additional intrinsic and extrinsic factors that cause the age-related decline of canonical Wnts and Wnt signaling remain elusive.

The intestine is an organ that harbors a vast collection of microbiota like bacteria, viruses, fungi, and protozoans (Hsiao et al., 2008). 16S rRNA sequencing and, more recently, shotgun sequencing analyses revealed a high level of complexity of microbial species in the intestine (Andersen et al., 2016; Janda and Abbott, 2007). Microbiota protect the host from the invasion of pathogenic microbes and support the maintenance of intestinal epithelium by regulating various signaling mechanisms that influence intestinal epithelial cells directly or indirectly through niche cells (Hou et al., 2017; Peck et al., 2017; Ubeda et al., 2017). The composition of the intestinal microbiota changes upon aging (Kumar et al., 2016). In older mice, the diversity of beneficial microbes decreases, while the population of pathogenic microbes increases. In aged humans, microbial diversity is lower compared to young (Kundu et al., 2017). These changes in microbial composition upon aging are thought to be one of the major causes of age-associated conditions like obesity (Sun et al., 2018), inflammatory

Published by Elsevier Inc. on behalf of International Society for Stem Cell Research.
This is an open access article under the CC BY-NC license (http://creativecommons.org/licenses/by-nc/4.0/).

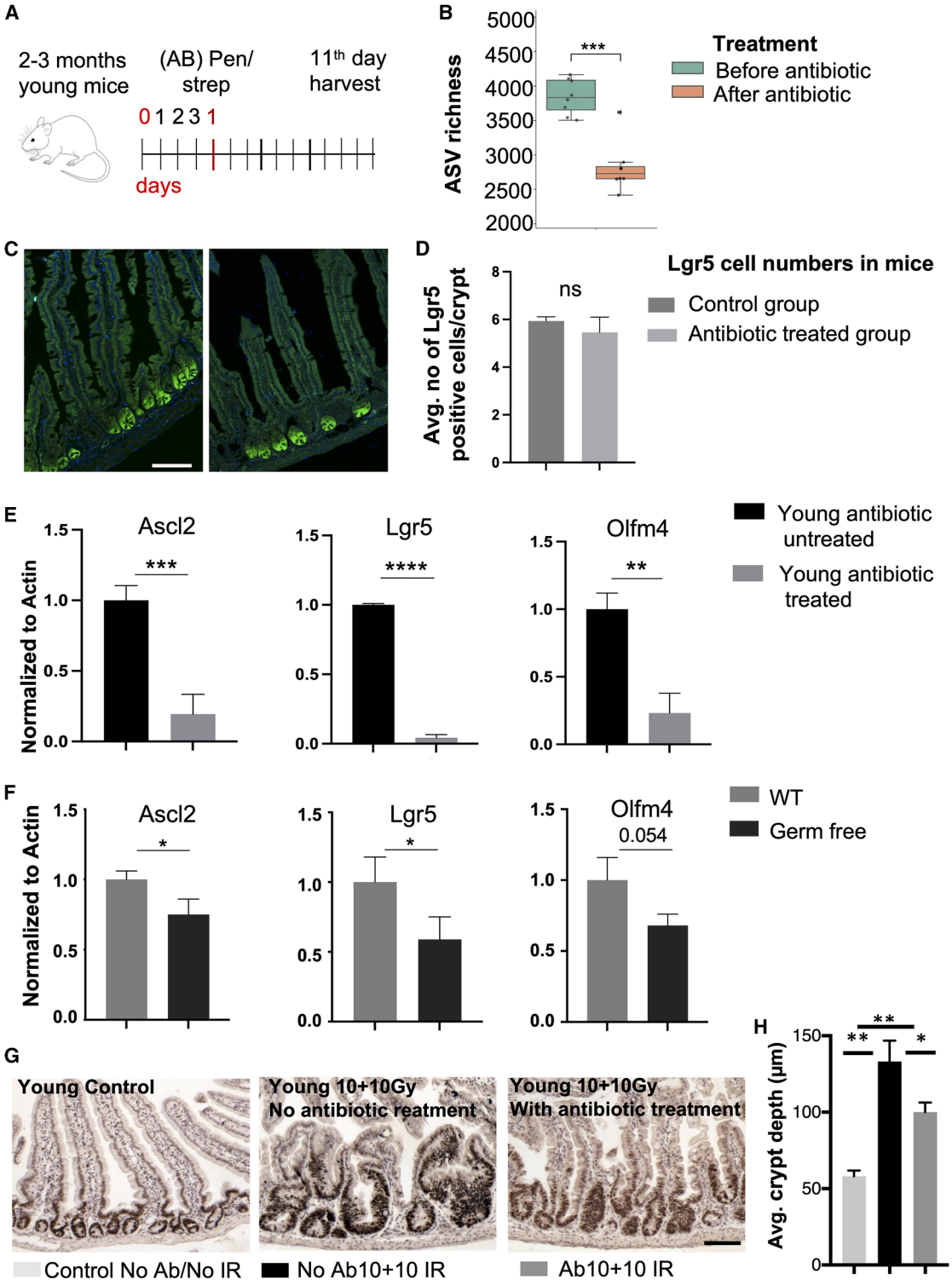


Figure 1. Microbiota modulates canonical Wnt signaling in intestinal stem cell crypts

(A) Experimental setup.

(B) Microbial load (amplicon sequence variant richness) in fecal samples with and without antibiotic treatment in 2- to 3-month-old mice.

(C) Representative picture of the proximal intestinal section of *Lgr5* EGFP mice with and without antibiotic treatment (scale bar, 100 µm).

(D) Average number of *Lgr5* GFP-positive cells/crypt.

(legend continued on next page)

bowel disease (Zuo and Ng, 2018), and irritable bowel syndrome (Theodorou et al., 2014).

Aging-associated changes in the composition of the microbiota might thus be targeted by oral administration of selected microbial species (pre-/probiotics) or by fecal microbiota trasfer (FMT) (Khoruts, 2018). For example, transplantation of young microbiota from the fish *Nothobranchius furzeri* to middle-aged *N. furzeri* enhanced the lifespan of the fish (Smith et al., 2017). Similarly, deletion of a set of 29 genes in *E. coli* increased the lifespan of their *C. elegans* host (Han et al., 2017). A more recent study demonstrated that FMT from wild-type mice enhanced the lifespan of progeroid mice (Barcena et al., 2019).

The role of microbial dysbiosis in modulating ISCs' function and canonical Wnt signaling in aged murine intestine remains poorly understood. In mice lacking commensal bacteria, evidence exists for reduced intestinal beta-catenin activity and at the same time, reduced levels of *Wnt5a* expression within murine colon tissue (Neumann et al., 2014). We demonstrate here that microbiota from young mice can enhance the regeneration of aged intestinal crypts *in vivo* by enhancing the aging-associated reduced *Ascl2*-driven Wnt signaling in ISCs. We further show that elevated levels of *Akkermansia muciniphila* in aged mice cause an attenuation of Wnt signaling and reduced regenerative function of aged ISCs *in vivo*. Aging-associated changes in the microbiota can thus be causatively linked to a reduced function of aged ISCs.

RESULTS

Microbiota modulates canonical Wnt signaling in intestinal stem cell crypts

Canonical Wnt signaling is critical for intestinal homeostasis (Pinto et al., 2003). To define the role of microbiota for Wnt signaling in intestine, we determined the level of expression of Wnt signaling genes in the crypts of animals treated with antibiotics or in germ-free (axenic) mice to investigate the extent to which depletion of microbiota results in changes in Wnt signaling. Antibiotic treatment of mice strongly reduced the levels of gut microbiota and changed its composition (Figures 1A and 1B). The number of ISCs (LGR5-EGFP cells) per crypt was not affected by the antibiotic treatment (Figures 1C and 1D). However, there was a reduced expression of the canonical Wnt signaling signature genes *Ascl2* and *Lgr5*, alongside a reduced expression of the ISC marker gene *Olfm4* in crypts from animals treated with antibiotics (Figure 1E) as well as in germ-free mice (Figure 1F). These data demonstrate that Wnt signaling in crypts is affected by the abundance of microbiota in the gut. These data are consistent with previous findings of reduced Wnt signaling in colonic crypts of mice (Neumann et al., 2014) and in zebrafish (Cheesman et al., 2011). Surprisingly, acute reduction of the level of microbiota in the antibiotic-treated animals resulted in a more extreme reduction of Wnt signaling in intestinal crypts compared to the chronic absence of microbiota in axenic mice. This more extreme decline in antibiotic treated mice might owe to the sudden loss of microbiota-derived signals that normally sustain high Wnt activity in conventional conditions. In contrast, germ-free mice inherently lack these microbial signals; thus, the baseline Wnt signaling is already low but remains sustained and likely derived from epithelial sources. The level of recovery of intestinal epithelium upon a 10 + 10 Gy irradiation (IR) allows to quantify the potential of ISCs to regenerate intestinal crypts (Nalapareddy and Geiger, 2020). In this assay, the average depth of the crypts serves as the marker for the level of the regenerative function of ISCs. There was a reduced average crypt depth in response to 10 + 10 Gy IR in mice treated with antibiotics (Figures 1G and 1H). These results demonstrate that changes in the composition of the microbiota can affect *Ascl2*-based Wnt signaling in ISCs as well as the regenerative function of ISCs.

Transfer of microbiota from young mice enhances canonical Wnt signaling in aged ISCs

There is a high level of variation among published data on the compositions of the gut microbiota, particularly with respect to the microbiota of aged mice. To confirm a distinct composition of microbiota in fecal samples from young and aged mice also in animals housed in our animal facility, fecal samples from young (2–3 months old) and aged (more than 18 months old) C57BL/6 animals was characterized by 16S ribosomal RNA sequencing (Figure 2A). Hierarchical cluster analysis (Figure S1A) and principal-component analysis (Figure S1B) confirmed distinct microbiota in fecal samples

(E) Relative level of expression of *Ascl2*, *Lgr5*, and *Olfm4* in crypts of antibiotic-treated and untreated control mice.
(F) Relative level of expression of *Ascl2*, *Lgr5*, and *Olfm4* in crypts of 2-month-old germ-free mice.
(G) Representative pictures of Ki67 staining used to measure viable, regenerative crypt depth in intestine from 2- to 3-months-old mice treated with antibiotics and in controls 5 days post 10 + 10 Gy irradiation.
(H) Crypt depth (in μm) in the proximal part of the intestine from mice treated with antibiotics and in controls 5 days post 10 + 10 Gy irradiation.
p values are determined by an unpaired *t* test with Welch's correction. $*p < 0.05$, $**p < 0.005$, $***p < 0.0005$. $n = 3–4$ mice/group. Error bars indicate Standard deviation.

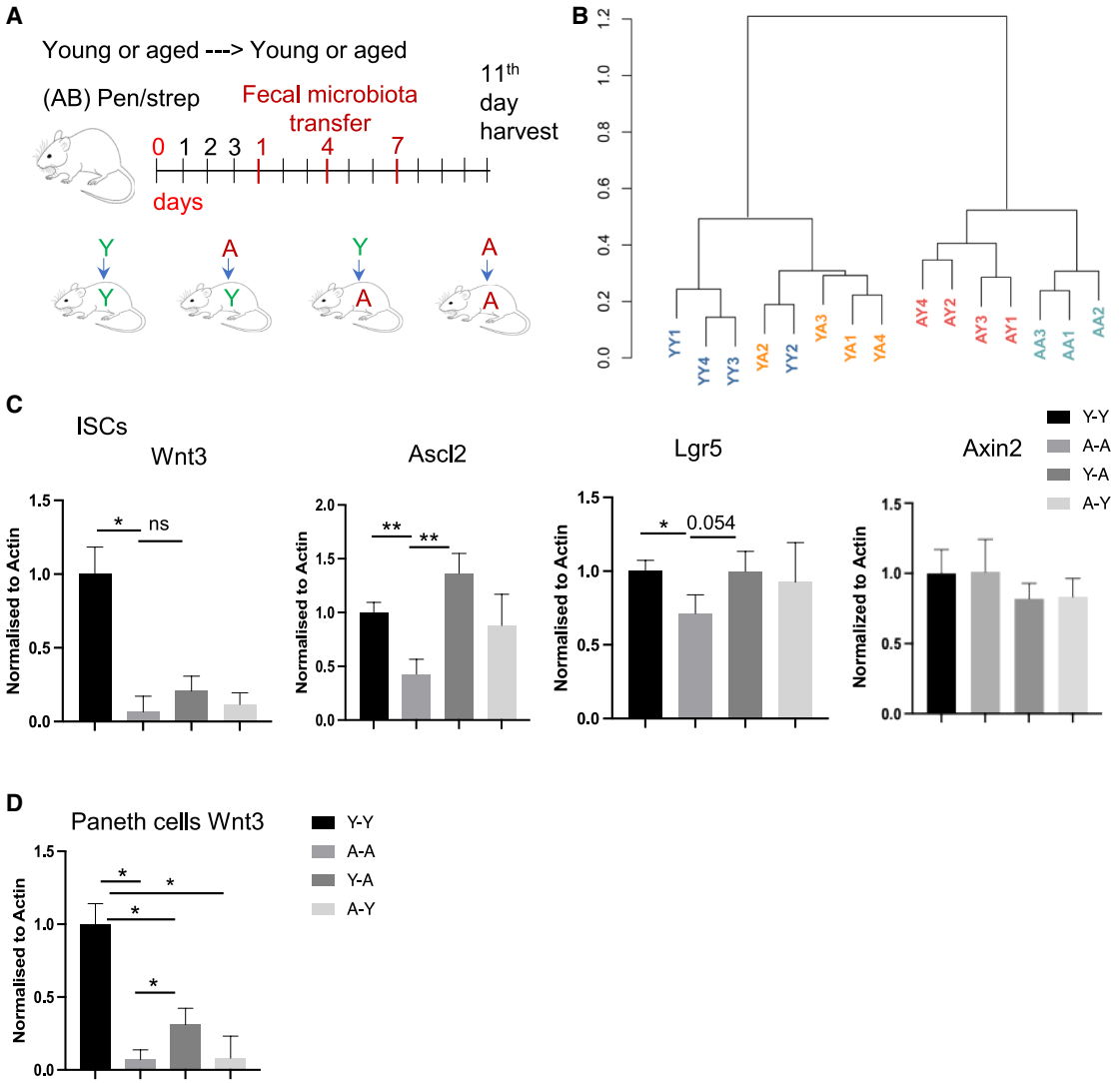


Figure 2. Transfer of microbiota from young mice enhances canonical Wnt signaling in aged ISCs

(A) Experimental setup.

(B) Hierarchical clustering analysis (unsupervised) on the composition of the microbiome in YY, YA, AY, and AA animals.

(C) Relative level of expression of *Wnt3*, *Ascl2*, *Lgr5*, and *Axin2* in LGR5+ cells from crypts from YY, YA, AY, and AA animals.

(D) Relative level of expression of *Wnt3* in Paneth cells of YY, YA, AY, and AA animals.

p values are determined by an unpaired *t* test with Welch's correction. $*p < 0.05$, $**p < 0.005$ ($n = 3–4$ mice per group). Error bars indicate Standard deviation.

from young and aged mice also within our animal facility (Kumar et al., 2016; Kundu et al., 2017).

Antibiotic treatment of aged animals resulted, as anticipated, in a decline of gut microbiota species richness (Figure S1C). We next performed heterochronic fecal microbial transfers ([FMTs]; YA: young to aged animals, and AY: aged to young animals) and accordingly homochronic control transfers (YY: young to young animals and AA: aged to aged animals) (Figure 2A). Both, hierarchical cluster analysis (Figure 2B) and principal-component analysis (Figure S1D) of microbial composition based on 16S ribosomal RNA sequencing of fecal samples from the animals 7 days post-transfer supported that heterochronic transfers resulted in a heterochronic contribution of the transferred fecal sample to the microbiota of the recipient animal, that is, YY and AA show the most distinct composition, with YA being distinct from AA and close to YY and AY being distinct from YY and more similar to AA (Figure 2B and S1D). These data demonstrate that the age of the transferred microbiota, at least under the conditions of

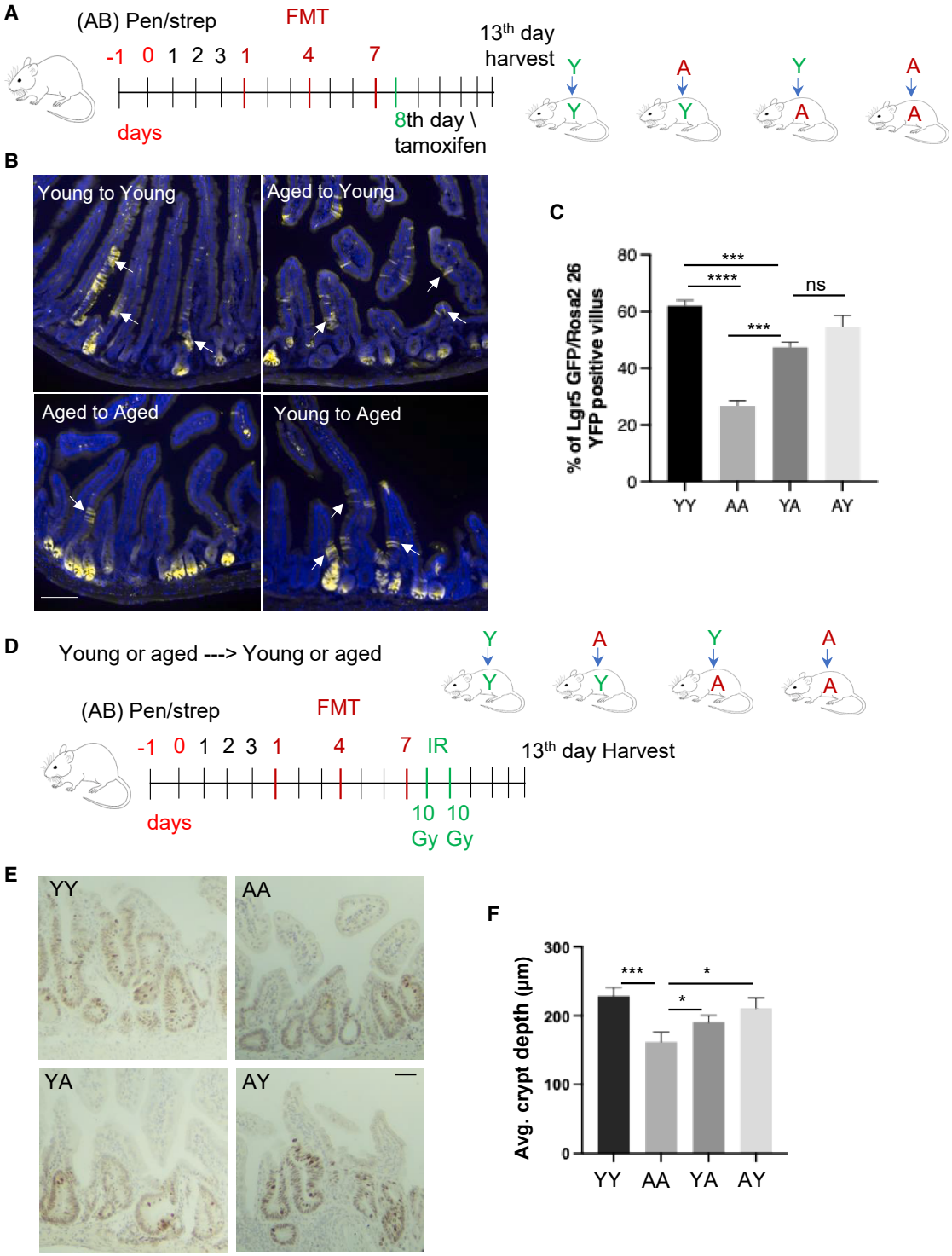


Figure 3. A young microbiota enhances the function of aged ISCs

(A) Experimental setup. Lineage tracing in young and aged *Lgr5*EGFPcreER Rosa26YFP mice upon *CreER* activation with tamoxifen.

(B) Representative images of YFP-positive crypts/villi harvested day 7 after FMT (day 5 after CreER induction; scale bar, 100 µm). Arrows indicate YFP positive cell in the villus.

(C) Percentage of YFP-positive villi/Lgr5YFP-positive crypts in the proximal part of YY, YA, AY, and AA animals. $*p < 0.05$, $**p < 0.005$, $***p < 0.0005$ ($n = 3$ mice/group).

(legend continued on next page)

FMT, affect the composition of the microbiota in the recipient, with the age clock of the microbiota in the intestine of the recipient animal set to the clock of the FMT donor.

We next evaluated the extent to which aged microbiota affect the level of canonical Wnt signaling in young and aged mouse intestinal crypts and ISCs from heterochronic and homochronic FMTs. Analyzing gene expression in homochronic transfers (YY vs. AA) identified that YY animals show higher levels of expression of *Wnt3* and of the canonical Wnt signaling genes *Ascl2* and *Lgr5* and higher level of the expression of the ISC marker gene *Olmf4* in crypts (Figure S1E) compared to AA animals. Similarly, there were higher levels of expression of *Wnt3*, *Ascl2*, and *Lgr5*, but not *Axin2*, in ISCs from YY compared to from AA animals (Figure 2C). In line with our previously published data (Nalapareddy et al., 2017), *Axin2* remains not linked to changes in Wnt signaling in aged ISCs, although playing a central role in Wnt signaling in other tissues (Nalapareddy et al., 2017). In both crypts and ISCs from young animals that received aged fecal samples (AY), the level of expression of *Wnt3* was significantly reduced (Figures 2C and S1E), while expression of *Ascl2*, *Lgr5*, *Axin2*, and *Olfm4* (Figures 2C and S1E) was only marginally reduced in comparison to homo-chronic young-young (YY) transfers. Most interestingly, aged animals that received young fecal samples (YA) showed significantly enhanced levels of expression of our indicator genes in crypts (Figure S1E), and for *Ascl2* and *Lgr5,* also in ISCs (Figure 2C), compared to aged animals that received aged microbiota (AA). These data demonstrate that the presence of young microbiota results in an elevated level of expression of a central canonical Wnt and Wnt signaling genes in aged crypts/ISCs, with the exception of *Axin2*, while transfer of an aged microbiota to young animals (AY) results in only marginal reduction of *Ascl2*-based canonical Wnt signaling in crypts/ISCs in the recipients. Paneth cells are niche cells for ISCs and secret canonical Wnts such as Wnt3 and other factors like NOTUM that can modulate cell-intrinsic canonical Wnt signaling in ISCs (Nalapareddy et al., 2017, 2022; Pentinmikko et al., 2019; Sato et al., 2011). In line with our data on the direction of changes in Wnt signaling in ISCs (Figure 2C), Paneth cells from YA animals showed an increase, although modest, in expression of *Wnt3* compared to cells from AA and AY animals (Figure 2D), while the transfer of aged fecal samples (AY) resulted in levels of *Wnt3* that were identical to the level in aged (AA) animals. In summary, these data support that aging-associated changes in microbiota can modulate *Ascl2*-based canonical Wnt signaling within aged ISCs but likely also by modulating Wnt3 in Paneth cells.

A young microbiota enhances the function of aged ISCs

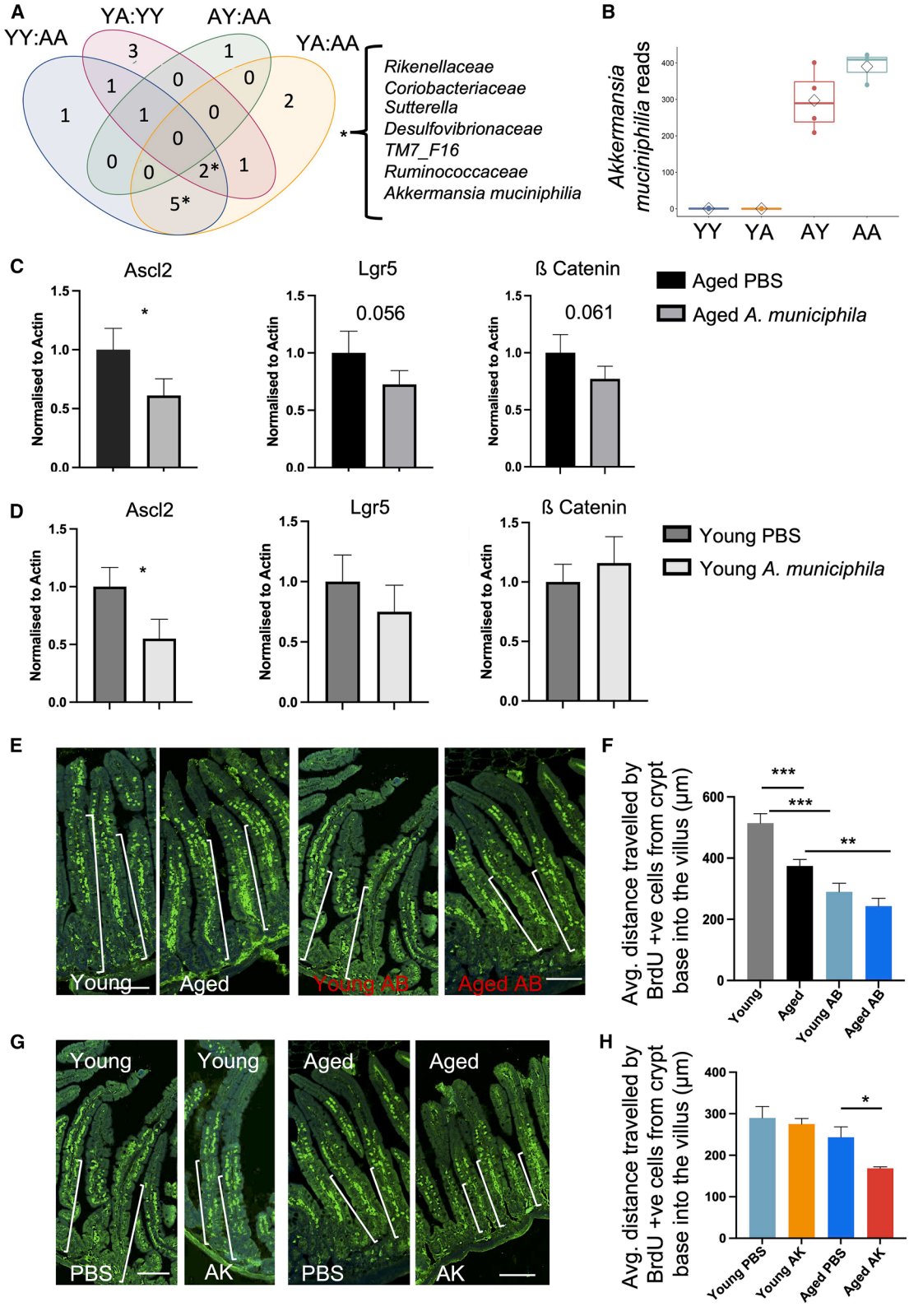
To determine the consequences of microbiota-induced changes in ISC signaling on ISC function, we performed lineage tracing experiments in *Lgr5-*$^{eGFP\text{-}IRES\text{-}CreERT2}$:*Rosa26*^{YFP} mice (Figure 3A). In these animals, YFP is activated in *Lgr5 Cre ERT2*-positive cells upon tamoxifen treatment. This will label ISCs and their offspring with YFP. Five days after FMT and after activation of YFP in ISCs, Lgr5/YFP-positive cells from crypts of YA animals presented with a higher percentage of YFP-positive cells in villi compared to villi from AA animals (Figures 3B and 3C). Supporting our observation of enhanced regeneration in YA animals, there was also an increase in the number of crypt cells undergoing mitosis in YA compared to AA animals (identified by staining against the phosphorylated form of histone H3 (pH3), (Figures S1F and S1G). These data show, consistent with the change in the *Wnt* gene expression profile, that there is an increase in the function of aged ISCs, resulting in enhanced regeneration of the intestinal epithelial tissue in the presence of young microbiota. Interestingly, AY animals showed only a marginally impaired regenerative response when compared to YY animals, which is in part consistent with a more modest effect of the aged microbiota on Wnt signaling in aged animals (Figures 3B and 3C). We also investigated whether changes in gut microbiota might further affect the number of ISC and Paneth cells. Quantification of ISCs, identified by the expression of *Olfm4*, an established ISC marker (Figures S1H and S1I), and Paneth cells, by expression of lysozyme (Figures S1J and S1K), indicated that FMTs do not affect the number of ISC or Paneth cells in young or aged mice.

Aged ISCs present with a reduced short-term regeneration in response to a 10 + 10 Gy radiation challenge (Nalapareddy and Geiger, 2020; Nalapareddy et al., 2017, 2021). To determine the level to which young microbiota is able to attenuate the stress-induced regenerative potential of aged ISCs, mice treated with antibiotics, followed by FMT, were subjected to 10 + 10 Gy radiation (Figure 3D). There was, as anticipated, an increase in the

(D) Experimental setup.

(E) Representative pictures of Ki67 staining used to measure viable, regenerative crypts in mouse intestine on day 4 after 10 + 10Gy irradiation.

(F) Crypt depth (in μm) in the proximal part of the intestine from mice on day 4 after 10 + 10 Gy irradiation. p values are determined by an unpaired t test with Welch's correction. $^{*}p < 0.05$, $^{***}p < 0.0005$. n = 3–4 mice/group. Error bars indicate Standard deviation.



(legend on next page)

average depth of the regenerating crypts in YY mice compared to AA mice at 4 days post-IR (Figures 3E and 3F). Strikingly, crypt regeneration in YA mice was significantly enhanced compared to crypts in AA mice. Similar to the result in lineage tracing experiment, there was only a marginal reduction in regeneration in AY compared to YY mice. The increase in the frequency of mitotic (pH3 positive) cells in crypts of YA compared to AA animals (Figures S1F and S1G) supported the notion of increased regeneration in YA compared to AA intestine. Together, these data demonstrate that young microbiota confers an enhanced and thus a more youthful regenerative potential on aged ISCs.

Elevated levels of *Akkermansia muciniphila* in aged animals cause attenuation of both *Ascl2*-based canonical Wnt signaling and ISC function

We next explored the possibility that individual species of microbiota that are differentially present in young and aged mice might modulate/effect Wnt signaling in ISCs. We, therefore, determined by 16S sequencing microbiota species that show a differential abundance among YY, AA, YA, and AA animals. Analysis of the data via Venn diagrams (Figure 4A) or bubble plots (Figures S2A and S2B) identified that YY vs. AA and YA vs. AA had 7 taxa in common, including *A. muciniphila* (Figures 4A, S2A, and S2B). The relative frequency of *A. muciniphila* was increased in the AY and AA groups compared to the YA or YY group (Figure 4B). While usually elevated levels of *A. muciniphila* are thought to be more beneficial for intestinal biology (Bell et al., 1986), *A. muciniphila* was previously also found to be reduced in centenarians (aka successful agers) (Wang et al., 2015). Elevated levels of *A. muciniphilia* might thus be also linked to negative effects. To characterize whether *A. muciniphila* can influence Wnt signaling in ISCs *in vivo*, young or aged mice received *A. muciniphila* (2×10^8 colony-forming units) via oral gavage (Figure S2C). While aged mice showed an increase in the relative frequency of *A. muciniphila* in the duodenum (determined by 16S sequencing) upon *A. muciniphila oral* gavage, the frequency of *A. muciniphila* in the duodenum of young animals was interestingly not affected by providing additional *A. muciniphila* (Figures S2D and S2E). *A. muciniphila* feeds on mucin produced in intestinal epithelium (Derrien et al., 2004). There are more mucin-producing goblet cells in the intestine of aged compared to young animals (Nalapareddy and Geiger, 2020; Nalapareddy et al., 2017). Aged mice might thus show elevated levels of mucin. It is thus a possibility that in young animals there is not enough mucin available to support elevated levels of *A. muciniphila* in this experimental setting.

The level of expression of the canonical Wnt signaling genes *Ascl2* and *Lgr5* was indeed further reduced in intestinal crypts from aged mice receiving *A. muciniphila* compared to age-matched controls (Figure 4C). Young mice, in accordance with the "no-change" of the level of *A. muciniphila* in *A. muciniphila*-treated mice (Figure S2D), showed no or only subtle changes in Wnt signaling (Figure 4D).

BrdU lineage tracing determines the distance of the migration of previously mitotic cells from the crypt base to the tip of the villus. It is another established assay to quantify the regenerative potential of ISCs *in vivo* (Ghaleb et al., 2011; Parker et al., 2017). This distance was reduced in antibiotic-treated young and aged mice (Figures 4E and 4F), further substantiating that changes in the microbiota affect ISC function (Figure 1). Second, there was a decline in the distance in aged *A. muciniphila*-treated mice compared to vehicle-treated mice (Figures 4G and 4H), which is in line with reduced canonical Wnt signaling in crypts of *A. muciniphila*-treated aged mice (Figure 4C). There was no difference in the distance in young animals treated with *A. muciniphila* compared to vehicle treatment,

Figure 4. Elevated levels of *Akkermansia muciniphila* in aged animals cause attenuation of both *Ascl2*-based canonical Wnt signaling and ISC function

(A) Venn analysis of the difference between the microbial taxa in the indicated FMT groups. "*" represents the groups in which microbial species or families enriched in young or aged animals after FMT.

(B) Frequency of reads of *A. muciniphila* upon FMT.

(C) Relative level of expression of *Ascl2*, *Lgr5*, and β-catenin in crypts of aged mice treated with *A. muciniphila* or vehicle.

(D) Relative level of expression of *Ascl2*, *Lgr5*, and β-catenin in crypts of young mice treated with *A. muciniphila* or vehicle.

(E) Representative pictures of stainings for BrdU lineage tracing in crypts of young and aged and young and aged AB-treated mice.

(F) Average distance traveled (from crypt base into the villus) by $BrdU^+$ cells in crypts of young and aged and young and aged AB-treated mice.

(G) Representative pictures of stainings for BrdU lineage tracing in young and aged mice treated with *A. muciniphila* or PBS after antibiotic treatment.

(H) Average distance traveled (from crypt base into the villus) by $BrdU^+$ cells in young and aged mice treated with *A. muciniphila* or PBS after antibiotic treatment. Note: young and aged AB (antibiotic)-treated mice in Figures 4E and 4F and Figures 4G and 4H young PBS and aged PBS after antibiotic treatment, treated with PBS are same.

p values are determined by an unpaired *t* test with Welch's correction. $*p < 0.05$, $**p < 0.005$, $***p < 0.0005$. $n = 3–4$ mice/group. Error bars indicate Standard deviation.

again likely due to the fact that levels of *A. muciniphila* did not change in the intestine in young animals upon providing additional amounts of *A. muciniphila* (Figure S2D). A decline of mitotic cells in aged crypts was also observed in young and aged mice (in line with previously published data (Nalapareddy et al., 2017) and in crypts from young and aged animals treated with antibiotics (Figures S3A and S3B). However, there was a further decline in the frequency of mitotic (pH3 positive) cells in crypts of aged *A. muciniphila* treated in comparison to aged control animals, but, as already anticipated, not in crypts of young animals (Figures S3C and S3D). These data are again consistent with a reduced regenerative potential of aged ISCs exposed to *A. muciniphila, as* determined by BrdU lineage tracing (Figures 4G and 4H).

We finally tested whether *A. muciniphila* affected the number of ISCs or their differentiation into Paneth cells. We observed no change in the frequency of ISCs (Olfm*4* positive cells) in young or aged crypts or crypts from animals treated with antibiotics or *A. muciniphila* (Figures S3E–S3H), which is in line with the observation that antibiotic treatment in young animals after FMT does not affect the number of Lgr5-positive cells. (Figures 1C and 1D). As previously reported (Nalapareddy et al., 2017; Pentinmikko et al., 2019), there is an increase in the frequency of Paneth (lysozyme positive) cells in the crypts of aged mice (Figures S3I and S3J). However, antibiotic treatment or *A. muciniphila* treatment did not affect the frequency of Paneth cells (Figures S3I–S3L).

Interestingly, along with the increase in *A. muciniphila* in the aged intestine upon feeding *A. muciniphila* (Figure S2E), there were significant changes in the frequency of other microbial species due to the elevated level of *A. muciniphila* (Figure S4). It thus remains a possibility that the change in function on ISCs upon the addition of *A. muciniphila* does not only stem only from *A. muciniphila* but also from the changes initiated by *A. muciniphila*, or that changes in multiple microbial species might be required to affect ISC function. For example, changes in the ratio of *A. muciniphila/ Lachnospiraceae* (A/L) (Lachnospiraceae are elevated upon AK (*Akkermansia muciniphila*) treatment, Figure S4) were reported to alter the microbial dynamics in gut (Chen et al., 2023). The frequency of *Bifidobacterium* as well as *Dubosiella* declined with *A. muciniphila* treatment (Figure S4). Both have been previously implied in reducing the permeability of the mucous layer (Yoshihara et al., 2020; Zhang et al., 2024).

In summary, our data indicate that increased amounts of a single species like *A. muciniphila* can be causative for attenuation of *Ascl2*- and *Lgr5*-mediated canonical Wnt signaling and reduced ISC function in aged mice, either by direct action on ISCs or via additional changes in the composition of the microbiota caused by an increase in the frequency of *A. muciniphila* in murine intestine. It is, therefore, also a possibility that only a combination of changes of metabolites secreted by several distinct species will affect Wnt signaling in ISCs or Paneth cells.

DISCUSSION

A decline in regenerative function of ISCs is one of the causes of reduced intestinal tissue homeostasis upon aging (Nalapareddy et al., 2017, 2022; Pentinmikko et al., 2019). We show here that aging-associated changes in microbiota can modulate *Ascl2*-based canonical Wnt signaling and the regenerative function of ISCs. Fecal microbiota transfer from young to aged mice, resulting in a more young-like microbiota in aged mice, restored *Ascl2* and *Lgr5* gene expression in crypts and ISCs and enhanced mitotic activity in crypts and the regenerative function of ISCs. The transfer of an aged microbiota to young mice only marginally affected Wnt signaling and the function of young ISCs. It is a possibility that young crypts are more resistant to acute changes in the relative composition of the microbiota compared to aged crypts. On the other hand, a strong reduction of the overall level of microbiota as in antibiotic-treated animals does significantly affect Wnt signaling and mitotic activity in young crypts. Microbiota-induced changes in signaling in intestine are also not confined to ISCs but are also seen in Paneth cells, the niche cells that secrete Wnt that supports ISC function.

In general, there is consensus in the field that there is a decrease in the abundance of *A. muciniphila* upon aging, while, however, several recent studies have found *A. muciniphila* to be significantly enriched in the gut of healthy and long-lived older adults (Zeng et al., 2023). On the other hand, *A. muciniphila* levels have been reported to be reduced in centenarians upon aging (Wang et al., 2015). Providing *A. muciniphila* to progeroid animals via gavage did extend lifespan (Barcena et al., 2019), which implies in this context a positive contribution of *A. muciniphila* to overall health. Overall, assigning changes in the abundance of a distinct species to an unequivocally negative or positive outcome with respect to aging-associated phenotypes is likely not possible.

In our FMT studies, the relative abundance of *A. muciniphila* was increased in aged animals that received aged microbiota (AA) when compared to young animals that received young microbiota (YY) and to aged animals that received young microbiota (AY). In our experiments, elevated levels of *A. muciniphila* negatively affected the level of canonical Wnt signaling, mitotic activity in crypts, and the regenerative potential of aged ISCs. The fact that providing *A. muciniphila* via gavage resulted only in aged mice in an increased representation of *A. muciniphila* in the intestine, but not in young mice, was unexpected but

might be explained by the lack of high levels of mucin in young mice. There is an increase in mucin-producing goblet cells in aged intestine (Nalapareddy et al., 2017, 2022; Pentinmikko et al., 2019), which might also explain the elevated abundance of *A. muciniphila in* AA animals, as *A. muciniphila* feeds on mucin. In general, though, this finding implies that simply providing additional levels of single species might not confer elevated levels of that species per se in the digestive track. It will be necessary to determine the overall composition of the microbiota in the section of interest of the digestive track with a special focus on the species provided. Our data further support that it is a possibility that only a combination of changes of metabolites secreted by several distinct species for which the abundance is affected in response to changes of an individual species like *A. muciniphila* will affect Wnt signaling in ISCs or Paneth cells.

In summary, our study demonstrates that aging-associated changes in the composition of the microbiota can modulate *Ascl2*-based canonical Wnt signaling in ISCs and, therefore, the regenerative potential of ISCs. Microbiota from young animals enhance *Ascl2*-based canonical Wnt signaling in aged ISCs and can be beneficial for the regenerative function of aged ISCs. The precise mechanisms by which microbiota modulate Wnt signaling requires further investigations.

METHODS

Mice

Young (2–3 months) C57BL/6 mice were purchased from Charles River, and aged mice (18–22 months) were obtained from the NIA colony. $Lgr5^{eGFPCreER(T2)}$ mice (Barker et al., 2007) and $Rosa26^{YFP}$ were purchased from Jackson Laboratories. $Lgr5^{eGFPCreER(T2)}$ mice were crossed with $Rosa26^{YFP}$ to obtain $Lgr5^{eGFPCreER(T2)}$ $Rosa26^{YFP}$, and animals were aged up to 2 years. All the data analysis on mouse intestine is from the proximal part of the mouse intestine unless otherwise indicated. All the mice were housed at CCHMC (Cincinnati Children's Hospital Medical Center) under specific pathogen-free conditions. Intestinal samples for crypt isolation were collected from 8-week-old germ-free mice. All animal experiments were approved by the Animal Care and Use Committee of Cincinnati Children's Hospital Medical Center.

Cultivation of *A. muciniphila*

Akkermansia muciniphila mucT (DSMZ-22959) were first inoculated from prepared cryo-preserved cultures into 5 mL *A. muciniphila* production medium (APM) (16 g/L peptone, 7 g/L yeast extract, 5 g/L NaCl, 1 g/L starch, 1 g/L glucose, 0.01% mucin) by an inoculation loop and incubated for 48 h at 37°C in anaerobic condition in Hungate tubes. After that, the bacteria precultures were prepared by transferring 500 μL of the previous culture in 5 mL new medium and incubated again at 37°C in anaerobic condition (90% N_2, 10% H_2) in Hungate tubes until the bacteria reached the beginning of the stationary growth phase. Subsequently, the main culture (250 mL) was inoculated to an OD_{600} of 0.1 and incubated at 37°C under anaerobic condition until the bacterium reached the end of exponential phase after 20 h. *A. muciniphila* was harvested in the desired growth phase, and portions of OD_{600} of 0.15 were centrifuged at 1,500 × *g* for 10 min. After that the cell pellet was resuspended in 50 μL Caso-Bouillon (30 g/L CASO-Bouillon; Carl Roth GmbH + Co. KG, Karlsruhe, Germany) supplemented with 10 g/L trehalose. The samples were stored overnight at −80°C prior to overnight drying in an Eppendorf vacuum Concentrator Plus (Eppendorf SE, Hamburg, Germany).

Crypts, ISCs, and Paneth cell isolation and gene expression analysis

For all analyses, the proximal part of the mouse small intestine was dissected and washed in cold PBS. Villi were removed by scraping the tissue with glass slides. Intestinal pieces were transferred to 5 mM EDTA in PBS (pH 8), followed by three times 1-min shaking by hand with a 10-min incubation at 4°C. Intestinal pieces were removed, centrifuged at 149 × *g* for 5 min, and the pellet was resuspended in PBS followed by centrifugation at 84 × *g* for 2 min. Crypts were incubated at 37°C in 4x TrypLE for 30–40 min on a rotor, washed twice with DMEM, centrifuged at 233 × *g* for 5 min, resuspended in 1 mL DMEM and incubated with CD24 PE (Phycoerythrin)-conjugated antibody for 30 min, washed with DMEM, filtered, and 7AAD was added; immediately the cells were subjected to 2-way sorting to collect GFP-positive ISCs and CD24PE-positive Paneth cells. Isolated crypt epithelial cells and ISCs and Paneth cells from the proximal part of the small intestine were used for gene expression analysis by quantitative reverse transcription PCR (RT-PCR). RNA was isolated using the Takara NucleoSpin Plus RNA isolation kit. Fifty nanograms of RNA were used per well in a single-step Taqman assay. Normalization was done using β-actin. FAM-labeled real-time PCR primers for mouse (ABI Applied Biosystems) were used.

Antibiotic treatment, fecal microbiota transfer (FMT), and oral gavage of *A. muciniphila*

Fecal samples were harvested a day before antibiotic treatment for both 16S rRNA sequencing and for preparing microbial suspension. 600 mg of fecal sample was dissolved in 9 mL of PBS, filtered through 70-μm filter and then with 40-μm filter, and 1 mL of glycerol (9 mL PBS + 1 mL glycerol) 10% glycerol in PBS) was added; aliquots were made and

stored at −80°C. After 3 days of antibiotic treatment, penicillin (2,000 U/mL) and streptomycin 2 mg/mL (Gibco), 200 μL of microbial suspension was given to mice via oral gavage, 3 times in total at an interval of 3 days. After last gavage, fecal samples were collected for sequencing and mice intestine were harvested for further analysis.

YFP (Yellow Fluorescent Protein) lineage tracing and 10 + 10 Gy irradiation

Young or aged mice (*Lgr5* CreERT2/R26YFP or C57BL/6 mice) were treated with antibiotics (pen/Step) for 3 days followed by FMT or transfer of *A. muciniphila* or PBS (vehicle) 3 times on alternative days via oral gavage. Mice were irradiated with 10 Gy on two consecutive days at the same time of the day 1 day after FMT or transfer of *A. muciniphila*. Murine proximal intestine was harvested on the fifth day after the first 10 Gy radiation. For *Lgr5*creERT2/R26YFP lineage tracing, 1 day after third AB treatment or FMT, mice were given tamoxifen for two consecutive days. Murine proximal intestine was harvested after 5–6 days, fixed in 4% paraformaldehyde, and washed in PBS after overnight incubation, followed by tissue processing and embedding. After a PBS wash, samples were further incubated in 30% sucrose overnight and mounted in blocks with the OCT (Optimal Cutting Temperature) compound and tissue sections (6 μM) prepared. Counting only Lgr5-positive crypts and villi showing YFP to determine the ratio of crypts that actively express GFP/YFP to villi showing YFP normalizes in this assay the mosaicism of the expression of Lgr5.

BrdU administration, anti-Olfm4, anti-phospho histone 3 (pH3), anti-lysozyme, anti-BrdU, and anti-Ki67 staining

Bromodeoxyuridine (BrdU) (Sigma-Aldrich) was injected at 100 mg/kg body weight. Murine proximal intestine was harvested 72 h after BrdU injection. 6-μm-thick paraffin-embedded tissue sections were deparaffinized; rehydrated; permeabilized by heating in 10 mM sodium citrate buffer; stained with BrdU primary antibody (Cell signaling, 1:100 dilution in PBS), Ki67 (Thermo Fisher, 1:100 dilution), pH3 (Cell Signaling, 1:100 dilution), LYSOZYME (Dako 1:400 dilution), and OLFM4 (1:100 dilution); incubated overnight at 4°C; and incubated with anti-mouse FITC-conjugated secondary antibody (Jackson ImmunoResearch Laboratories, 1:200 dilution (both for BrdU and Olfm4 stainings) for 1 h at room temperature or 1:200 anti-mouse biotinylated antibody followed by ABC kit (Vector Shields) or anti-rabbit Cy3-conjugated secondary antibody (Jackson ImmunoReseach Laboratories, 1:200 [for pH3 and lysozyme stainings]). Pictures were taken under 10x or 20x magnification (both with a confocal and a regular microscope). The distance of the midpoint of BrdU-positive cells to the crypt base was measured using ImageJ software.

UNC microbiome core 16S rRNA isolation and analysis

Stool sample DNA Isolation

Samples were transferred to a 2-mL tube containing 200 mg of ≤106-μm glass beads (Sigma, St. Louis, MO) and 0.5 mL of Qiagen PM1 buffer (Valencia, CA). Bead beating was performed for 5-min in a Qiagen TissueLyser II at 30Hz. After a 5-min centrifugation, 0.45 mL of supernatant was aspirated and transferred to a new tube containing 0.15 mL of Qiagen IRS solution. The suspension was incubated at 4°C overnight. After a brief centrifugation, supernatants were aspirated and transferred to deep-well plates containing 0.45 mL of Qiagen binding buffer supplemented with Qiagen ClearMag Beads. DNA was purified using the automated KingFisherTM Flex Purification System and eluted in DNase-free water (Allali et al., 2017; Azcarate-Peril et al., 2018; Guadamuro et al., 2019).

16S rRNA amplicon sequencing

12.5 ng of total DNA were amplified using universal primers targeting the V4 region of the bacterial 16S rRNA gene1, 2. Primer sequences contained overhang adapters appended to the 5′ end of each primer for compatibility with Illumina sequencing platform. The primers used were F515/R806 (Caporaso et al., 2011). Master mixes contained 12.5 ng of total DNA, 0.5 μM of each primer, and 2x KAPA HiFi HotStart ReadyMix (KAPA Biosystems, Wilmington, MA). The thermal profile for the amplification of each sample had an initial denaturing step at 95°C for 3 min, followed by a cycling of denaturing of 95°C for 30 s, annealing at 55°C for 30 s and a 30-s extension at 72°C (25 cycles), a 5-min extension at 72°C, and a final hold at 4°C. Each 16S amplicon was purified using the AMPure XP reagent (Beckman Coulter, Indianapolis, IN). In the next step, each sample was amplified using a limited cycle PCR program, adding Illumina sequencing adapters and dual-index barcodes (index 1(i7) and index 2(i5)) (Illumina, San Diego, CA) to the amplicon target. The thermal profile for the amplification of each sample had an initial denaturing step at 95°C for 3 min, followed by a denaturing cycle of 95°C for 30 s, annealing at 55°C for 30 s and a 30-s extension at 72°C (8 cycles), a 5-min extension at 72°C, and a final hold at 4°C. The final libraries were again purified using the AMPure XP reagent (Beckman Coulter), quantified, and normalized prior to pooling. The DNA library pool was then denatured with NaOH, diluted with hybridization buffer, and heat denatured before loading on the MiSeq reagent cartridge (Illumina) and on the MiSeq instrument (Illumina). Automated cluster generation and paired-end sequencing with dual reads were performed according to the manufacturer's instructions.

Bioinformatics analysis

Sequencing output from the Illumina MiSeq platform was converted to fastq format and demultiplexed using Illumina Bcl2Fastq 2.18.0.12. The resulting paired-end reads were processed using QIIME 2 2018.11(Mohsen et al., 2019). Index and linker primer sequences were trimmed using the QIIME 2 invocation of cutadapt. The resulting paired-end reads were processed with DADA2 through QIIME 2 including merging paired ends, quality filtering, error correction, and chimera detection (Callahan et al., 2016). Amplicon sequencing units from DADA2 were assigned taxonomic identifiers with respect to Green Genes release 13_08 using the QIIME 2 q2-feature classifier (Bokulich et al., 2018). Alpha diversity with respect to Faith PD whole tree, Evenness (Shannon) index, and observed species number metrics was estimated using QIIME 2 at a rarefaction depth of 5,000 sequences per subsample. Beta diversity estimates were calculated within QIIME 2 using weighted and unweighted Unifrac distances as well as Bray-Curtis dissimilarity between samples at a subsampling depth of 5,000. Results were summarized and visualized through principal coordinate analysis, and significance was estimated as implemented in QIIME 2. Significance of differential abundance was estimated using AnCom as implemented in QIIME 2.

Microbiome data analysis of young, aged, YY, YA, AY, and AA groups

Taxonomic count data were processed as follows. First, unassigned reads were removed. Next, reads counts were normalized across samples by rarefaction using the command rrarefy from the Vegan package in R. Hierarchical clustering was performed on log2 transformed data using the vegdist and hclust commands from the Vegan package in R. A Venn diagram demonstrating taxa that overlapped between mouse groups was generated using the draw.quad.venn command from the VennDiagram package in R. Principal-component analysis was performed on generalized log2 scaled count data using the command PCA from the factoMineR package in R. Bubble plots were generated from count data using Tableau.

BIOMES 16S sequencing and analysis

Sample processing, sample storage. and lysis

Collected stool samples are stored in up to 1,000 μL DNA-stabilizing buffer at −20°C until use. For the lysis process, the samples are defrosted and centrifuged at 4,000 × *g* for 15 min. Afterward, 650 μL of warmed up lysis buffer was added to each sample, and then vortexed for 20 min.

Extraction of stool samples

Afterward, we extract the nucleic acid on our liquid handling systems (*Hamilton StarLine*) by using a vacuum chamber as well as a high-pressure chamber. The extracted gDNA (genomicDNA) is stored at −20°C until use.

Library preparation for sequencing with the Illumina NextSeq2000 system

The library preparation follows the manual "16S Metagenomic Sequencing Library Preparation- Preparing 16S Ribosomal RNA Gene Amplicons for the Illumina MiSeq System." For normalization of all samples, a fluorescent dye and the Biotek Synergy HTX plate reader are used to measure DNA concentrations and to calculate the necessary dilution volume per sample. All the steps described are nearly fully automated by using our liquid handling systems (Hamilton StarLine). Hence, we can process multiple samples simultaneously. The library denaturing and NextSeq2000 sample loading are carried out automatically following the Illumina protocol NextSeq 1000/2000 Product Documentation. Demultiplexing is performed directly on the NextSeq after sequencing, and the resulting FastQ-files are generated for subsequent data analysis.

Processing and analysis of sequence data

The paired-end reads from NextSeq (2 × 300 cycles) are merged to reconstruct overlapping sequences with 430–460 base length. Chimera und borderline reads are filtered out with usearch uchime2_ref tool (Edgar, 2016). SILVA 138.1 is used as database for usearch uchime (NCBI Insights, 2019). For taxonomic alignment, Amplicon sequence variants (ASVs) are determined using BLASTn (Nucleotide-Nucleotide BLAST 2.10.1+) (NCBI Insights, 2019) against SILVA 138.1 (Quast et al., 2013). Alignment Identity must meet a threshold of at least Phylum: 75.0, Class: 78.5, Order: 82.4, Family: 86.5, Genus: 94.5, Species: 97.0. RefSeqs/Counts tables are created for all samples using Python package Pandas 1.3.4 (Reback, 2022). The taxonomic composition of microbial communities is inferred from ASV counts at the phylum, genus, and species levels.

Copy number normalization

Further bioinformatic analyses are done using Picrust2 (Douglas et al., 2020). The study sequences of the alignment step are placed into a reference tree to determine/predict the copy numbers and the NSTI-index (nearest-sequenced taxon index). All study sequences with NSTI-index higher than 2 are excluded.

Summary of downstream analysis

Statistical methods	Visualization methods	Python packages
Independent and paired *t* tests	Bar graphs	scipy
ANOVA (analysis of variance)	Boxplots	statsmodels
		seaborn, matplotlib

Statistical analyses

To calculate statistical significance, either a Student's *t* test or a Wilcoxon/Mann-Whitney test was used. Error bars indicate SD. GraphPad Prism or Microsoft Excel was used for statistical analyses.

RESOURCE AVAILABILITY

Lead contact

Requests for further information and resources should be directed to and will be fulfilled by the lead contact, Hartmut Geiger (hartmut.geiger@uni-ulm.de).

Materials availability

This study did not generate new unique reagents.

Data and code availability

- For the data generated at UNC: SRA archive, accession number PRJNA1358964 https://www.ncbi.nlm.nih.gov/sra/?term=PRJNA1358964 PRJNA1358964; for the data generated at BIOMES: https://dataverse.harvard.edu/dataset.xhtml?persistentId = doi:10.7910/DVN/UHQAHA) was published in Geigerlab Dataverse (view at https://dataverse.harvard.edu/dataverse/Geigerlab).
- Any additional information required to reanalyze the data reported in this paper is available from the lead contact upon request. Original microscopy data and real-time RT-PCR data reported in this paper will be shared by the lead contact upon request.

ACKNOWLEDGMENTS

We thank the flow core and the Comprehensive Mouse and Cancer Core at CCHMC. We thank BIOMES NGS GmbH, Wildau, Germany for 16S sequencing and data analysis. We also thank the UNC Microbiome core for 16S Ribosomal RNA sequencing. Work in the laboratory was supported by grants from the NIH (R01DK104814, R01AG063967, P30DK078392, and AG040118). This work was further financed by the Baden-Württemberg Stiftung in the project MIKROBIOM: ID23 AMDA.

AUTHOR CONTRIBUTIONS

K.N. performed all the experiments. D.B.H performed bioinformatic analysis of 16S rRNA sequencing and data interpretation. Y.Z. helped in data interpretation, T.A. provided germ-free mice for experiments. F.R and A.-K.K. provided *A. muciniphila* cultures for experiments. S.S helped with sample submission for rRNA sequencing of microbiota. K.N., Y.Z., and H.G. conceived the project, designed the experiments, and wrote the manuscript.

DECLARATION OF INTERESTS

The authors declare no competing interests.

SUPPLEMENTAL INFORMATION

Supplemental information can be found online at https://doi.org/10.1016/j.stemcr.2025.102788.

Received: May 7, 2025
Revised: December 22, 2025
Accepted: December 23, 2025
Published: January 22, 2026

REFERENCES

Allali, I., Arnold, J.W., Roach, J., Cadenas, M.B., Butz, N., Hassan, H.M., Koci, M., Ballou, A., Mendoza, M., Ali, R., and Azcarate-Peril, M.A. (2017). A comparison of sequencing platforms and bioinformatics pipelines for compositional analysis of the gut microbiome. BMC Microbiol. *17*, 194. https://doi.org/10.1186/s12866-017-1101-8.

Andersen, H., Connolly, N., Bangar, H., Staat, M., Mortensen, J., Deburger, B., and Haslam, D.B. (2016). Use of Shotgun Metagenome Sequencing To Detect Fecal Colonization with Multidrug-Resistant Bacteria in Children. J. Clin. Microbiol. *54*, 1804–1813. https://doi.org/10.1128/JCM.02638-15.

Azcarate-Peril, M.A., Butz, N., Cadenas, M.B., Koci, M., Ballou, A., Mendoza, M., Ali, R., and Hassan, H. (2018). An Attenuated Salmonella enterica Serovar Typhimurium Strain and Galacto-Oligosaccharides Accelerate Clearance of Salmonella Infections in Poultry through Modifications to the Gut Microbiome. Appl. Environ. Microbiol. *84*, e02526-17. https://doi.org/10.1128/AEM.02526-17.

Barcena, C., Valdes-Mas, R., Mayoral, P., Garabaya, C., Durand, S., Rodriguez, F., Fernandez-Garcia, M.T., Salazar, N., Nogacka, A.M., Garatachea, N., et al. (2019). Healthspan and lifespan extension by fecal microbiota transplantation into progeroid mice. Nat. Med. *25*, 1234–1242. https://doi.org/10.1038/s41591-019-0504-5.

Barker, N., van Es, J.H., Kuipers, J., Kujala, P., van den Born, M., Cozijnsen, M., Haegebarth, A., Korving, J., Begthel, H., Peters, P.J., and Clevers, H. (2007). Identification of stem cells in small intestine and colon by marker gene Lgr5. Nature *449*, 1003–1007. https://doi.org/10.1038/nature06196.

Bell, J.L., McNeill, D.P., Dandona, P., and Wojdyla, J.W. (1986). Immunoturbidimetric assay of slight albuminuria with a centrifugal analyzer. Clin. Chem. *32*, 1412.

Bokulich, N.A., Kaehler, B.D., Rideout, J.R., Dillon, M., Bolyen, E., Knight, R., Huttley, G.A., and Gregory Caporaso, J. (2018). Optimizing taxonomic classification of marker-gene amplicon sequences with QIIME 2's q2-feature-classifier plugin. Microbiome *6*, 90. https://doi.org/10.1186/s40168-018-0470-z.

Callahan, B.J., McMurdie, P.J., Rosen, M.J., Han, A.W., Johnson, A.J.A., and Holmes, S.P. (2016). DADA2: High-resolution sample inference from Illumina amplicon data. Nat. Methods *13*, 581–583. https://doi.org/10.1038/nmeth.3869.

Caporaso, J.G., Lauber, C.L., Walters, W.A., Berg-Lyons, D., Lozupone, C.A., Turnbaugh, P.J., Fierer, N., and Knight, R. (2011). Global patterns of 16S rRNA diversity at a depth of millions of sequences per sample. Proc. Natl. Acad. Sci. USA *108*, 4516–4522. https://doi.org/10.1073/pnas.1000080107.

Cheesman, S.E., Neal, J.T., Mittge, E., Seredick, B.M., and Guillemin, K. (2011). Epithelial cell proliferation in the developing zebrafish intestine is regulated by the Wnt pathway and microbial signaling via Myd88. Proc. Natl. Acad. Sci. USA *108*, 4570–4577. https://doi.org/10.1073/pnas.1000072107.

Chen, P.C., Lin, M.S., Lin, T.C., Kang, T.W., and Ruan, J.W. (2023). The Alteration of Akkermansiaceae/Lachnospiraceae Ratio Is a Microbial Feature of Antibiotic-Induced Microbiota Remodeling. Bioinform. Biol. Insights *17*, 11779322231166229. https://doi.org/10.1177/11779322231166229.

Derrien, M., Vaughan, E.E., Plugge, C.M., and de Vos, W.M. (2004). Akkermansia muciniphila gen. nov., sp. nov., a human intestinal mucin-degrading bacterium. Int. J. Syst. Evol. Microbiol. *54*, 1469–1476. https://doi.org/10.1099/ijs.0.02873-0.

Douglas, G.M., Maffei, V.J., Zaneveld, J., Yurgel, S.N., Brown, J.R., Taylor, C.M., Huttenhower, C., and Langille, M.G.I. (2020). PICRUSt2: An improved and customizable approach for metagenome inference. Preprint at bioRxiv. https://doi.org/10.1101/672295.

Edgar, R.C. (2016). UCHIME2: improved chimera prediction for amplicon sequencing. Preprint at bioRxiv. https://doi.org/10.1101/074252.

Ghaleb, A.M., McConnell, B.B., Kaestner, K.H., and Yang, V.W. (2011). Altered intestinal epithelial homeostasis in mice with intestine-specific deletion of the Kruppel-like factor 4 gene. Dev. Biol. *349*, 310–320. https://doi.org/10.1016/j.ydbio.2010.11.001.

Guadamuro, L., Azcárate-Peril, M.A., Tojo, R., Mayo, B., and Delgado, S. (2019). Use of high throughput amplicon sequencing and ethidium monoazide dye to track microbiota changes in an equol-producing menopausal woman receiving a long-term isoflavones treatment. AIMS Microbiol. *5*, 102–116. https://doi.org/10.3934/microbiol.2019.1.102.

Han, B., Sivaramakrishnan, P., Lin, C.C.J., Neve, I.A.A., He, J., Tay, L.W.R., Sowa, J.N., Sizovs, A., Du, G., Wang, J., et al. (2017). Microbial Genetic Composition Tunes Host Longevity. Cell *169*, 1249–1262.e13. https://doi.org/10.1016/j.cell.2017.05.036.

He, D., Wu, H., Xiang, J., Ruan, X., Peng, P., Ruan, Y., Chen, Y.G., Wang, Y., Yu, Q., Zhang, H., et al. (2020). Gut stem cell aging is driven by mTORC1 via a p38 MAPK-p53 pathway. Nat. Commun. *11*, 37. https://doi.org/10.1038/s41467-019-13911-x.

Hou, Q., Ye, L., Huang, L., and Yu, Q. (2017). The Research Progress on Intestinal Stem Cells and Its Relationship with Intestinal Microbiota. Front. Immunol. *8*, 599. https://doi.org/10.3389/fimmu.2017.00599.

Hsiao, W.W.L., Metz, C., Singh, D.P., and Roth, J. (2008). The microbes of the intestine: an introduction to their metabolic and signaling capabilities. Endocrinol. Metab. Clin. North Am. *37*, 857–871. https://doi.org/10.1016/j.ecl.2008.08.006.

Janda, J.M., and Abbott, S.L. (2007). 16S rRNA gene sequencing for bacterial identification in the diagnostic laboratory: pluses, perils, and pitfalls. J. Clin. Microbiol. *45*, 2761–2764. https://doi.org/10.1128/JCM.01228-07.

Khoruts, A. (2018). Targeting the microbiome: from probiotics to fecal microbiota transplantation. Genome Med. *10*, 80. https://doi.org/10.1186/s13073-018-0592-8.

Kumar, M., Babaei, P., Ji, B., and Nielsen, J. (2016). Human gut microbiota and healthy aging: Recent developments and future prospective. Nutr. Healthy Aging *4*, 3–16. https://doi.org/10.3233/NHA-150002.

Kundu, P., Blacher, E., Elinav, E., and Pettersson, S. (2017). Our Gut Microbiome: The Evolving Inner Self. Cell *171*, 1481–1493. https://doi.org/10.1016/j.cell.2017.11.024.

Mohsen, A., Park, J., Chen, Y.-A., Kawashima, H., and Mizuguchi, K. (2019). Impact of quality trimming on the efficiency of reads joining and diversity analysis of Illumina paired-end reads in the context of QIIME1 and QIIME2 microbiome analysis frameworks. BMC Bioinf. *20*, 581. https://doi.org/10.1186/s12859-019-3187-5.

Nalapareddy, K., and Geiger, H. (2020). Analysis of Aged Dysfunctional Intestinal Stem Cells. Methods Mol. Biol. *2171*, 41–52. https://doi.org/10.1007/978-1-0716-0747-3_3.

Nalapareddy, K., Hassan, A., Sampson, L.L., Zheng, Y., and Geiger, H. (2021). Suppression of elevated Cdc42 activity promotes the regenerative potential of aged intestinal stem cells. iScience *24*, 102362. https://doi.org/10.1016/j.isci.2021.102362.

Nalapareddy, K., Nattamai, K.J., Kumar, R.S., Karns, R., Wikenheiser-Brokamp, K.A., Sampson, L.L., Mahe, M.M., Sundaram, N., Yacyshyn, M.B., Yacyshyn, B., et al. (2017). Canonical Wnt Signaling Ameliorates Aging of Intestinal Stem Cells. Cell Rep. *18*, 2608–2621. https://doi.org/10.1016/j.celrep.2017.02.056.

Nalapareddy, K., Zheng, Y., and Geiger, H. (2022). Aging of intestinal stem cells. Stem Cell Rep. *17*, 734–740. https://doi.org/10.1016/j.stemcr.2022.02.003.

NCBI Insights (2019). BLAST+ 2.10.0 now available with improved composition-based statistics.

Neumann, P.A., Koch, S., Hilgarth, R.S., Perez-Chanona, E., Denning, P., Jobin, C., and Nusrat, A. (2014). Gut commensal bacteria and regional Wnt gene expression in the proximal versus distal colon. Am. J. Pathol. *184*, 592–599. https://doi.org/10.1016/j.ajpath.2013.11.029.

Parker, A., Maclaren, O.J., Fletcher, A.G., Muraro, D., Kreuzaler, P.A., Byrne, H.M., Maini, P.K., Watson, A.J.M., and Pin, C. (2017). Cell proliferation within small intestinal crypts is the principal driving force for cell migration on villi. FASEB J. *31*, 636–649. https://doi.org/10.1096/fj.201601002.

Peck, B.C.E., Shanahan, M.T., Singh, A.P., and Sethupathy, P. (2017). Gut Microbial Influences on the Mammalian Intestinal Stem Cell Niche. Stem Cells Int. *2017*, 5604727. https://doi.org/10.1155/2017/5604727.

Pentinmikko, N., Iqbal, S., Mana, M., Andersson, S., Cognetta, A.B., Suciu, R.M., Roper, J., Luopajärvi, K., Markelin, E., Gopalakrishnan, S., et al. (2019). Notum produced by Paneth cells attenuates regeneration of aged intestinal epithelium. Nature *571*, 398–402. https://doi.org/10.1038/s41586-019-1383-0.

Pinto, D., Gregorieff, A., Begthel, H., and Clevers, H. (2003). Canonical Wnt signals are essential for homeostasis of the intestinal epithelium. Genes Dev. *17*, 1709–1713. https://doi.org/10.1101/gad.267103.

Quast, C., Pruesse, E., Yilmaz, P., Gerken, J., Schweer, T., Yarza, P., Peplies, J., and Glöckner, F.O. (2013). The SILVA ribosomal RNA gene database project: improved data processing and web-based tools. Nucleic Acids Res. *41*, D590–D596. https://doi.org/10.1093/nar/gks1219.

Reback, J. (2022). Pandas-Dev/Pandas: . Nucleic Acids Res Pandas*1* (Zenodo).

Sato, T., van Es, J.H., Snippert, H.J., Stange, D.E., Vries, R.G., van den Born, M., Barker, N., Shroyer, N.F., van de Wetering, M., and Clevers, H. (2011). Paneth cells constitute the niche for Lgr5 stem cells in intestinal crypts. Nature *469*, 415–418. https://doi.org/10.1038/nature09637.

Smith, P., Willemsen, D., Popkes, M., Metge, F., Gandiwa, E., Reichard, M., and Valenzano, D.R. (2017). Regulation of life span by the gut microbiota in the short-lived African turquoise killifish. eLife *6*, e27014. https://doi.org/10.7554/eLife.27014.

Sun, L., Ma, L., Ma, Y., Zhang, F., Zhao, C., and Nie, Y. (2018). Insights into the role of gut microbiota in obesity: pathogenesis, mechanisms, and therapeutic perspectives. Protein Cell *9*, 397–403. https://doi.org/10.1007/s13238-018-0546-3.

Theodorou, V., Ait Belgnaoui, A., Agostini, S., and Eutamene, H. (2014). Effect of commensals and probiotics on visceral sensitivity and pain in irritable bowel syndrome. Gut Microbes. *5*, 430–436. https://doi.org/10.4161/gmic.29796.

Ubeda, C., Djukovic, A., and Isaac, S. (2017). Roles of the intestinal microbiota in pathogen protection. Clin. Transl. Immunology *6*, e128. https://doi.org/10.1038/cti.2017.2.

Wang, F., Yu, T., Huang, G., Cai, D., Liang, X., Su, H., Zhu, Z., Li, D., Yang, Y., Shen, P., et al. (2015). Gut Microbiota Community and Its Assembly Associated with Age and Diet in Chinese Centenarians. J. Microbiol. Biotechnol. *25*, 1195–1204. https://doi.org/10.4014/jmb.1410.10014.

Yoshihara, T., Oikawa, Y., Kato, T., Kessoku, T., Kobayashi, T., Kato, S., Misawa, N., Ashikari, K., Fuyuki, A., Ohkubo, H., et al. (2020). The protective effect of Bifidobacterium bifidum G9-1 against mucus degradation by Akkermansia muciniphila following small intestine injury caused by a proton pump inhibitor and aspirin. Gut Microbes. *11*, 1385–1404. https://doi.org/10.1080/19490976.2020.1758290.

Zeng, S.Y., Liu, Y.F., Liu, J.H., Zeng, Z.L., Xie, H., and Liu, J.H. (2023). Potential Effects of Akkermansia Muciniphila in Aging and Aging-Related Diseases: Current Evidence and Perspectives. Aging Dis. *14*, 2015–2027. https://doi.org/10.14336/AD.2023.0325.

Zhang, Y., Tu, S., Ji, X., Wu, J., Meng, J., Gao, J., Shao, X., Shi, S., Wang, G., Qiu, J., et al. (2024). Dubosiella newyorkensis modulates immune tolerance in colitis via the L-lysine-activated AhR-IDO1-Kyn pathway. Nat. Commun. *15*, 1333. https://doi.org/10.1038/s41467-024-45636-x.

Zuo, T., and Ng, S.C. (2018). The Gut Microbiota in the Pathogenesis and Therapeutics of Inflammatory Bowel Disease. Front. Microbiol. *9*, 2247. https://doi.org/10.3389/fmicb.2018.02247.